ACS Catalysis

Review

pubs.acs.org/acscatalysis

Advanced Platinum Alloy Electrocatalysts for the Oxygen Reduction Reaction

Chao Wang, Nenad M. Markovic, and Vojislav R. Stamenkovic*

Materials Science Division, Argonne National Laboratory, Argonne, Illinois 60439, United States

ABSTRACT: In the past decade, significant advancement has been made in the development of electrocatalysts for energy conversion and storage. Among various approaches, alloying Pt with 3d transition metals has shown great potential in tailoring the atomic and electronic structures of catalytically active materials toward improved catalytic performance. Here, we provide a brief overview of the recent advancements in the design and synthesis of electrocatalysts for the oxygen reduction reaction. Our focus is placed on the systematic studies of particle size, composition, and shape effect for the monodisperse and homogeneous platinum alloy electrocatalysts that have been synthesized by organic solution approaches.

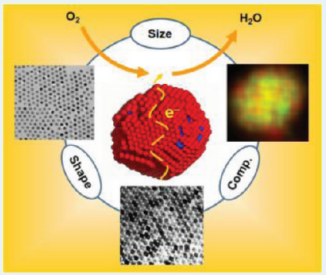

KEYWORDS: *platinum, alloy, electrocatalysts, oxygen reduction reaction*

INTRODUCTION

Alloys have attracted increasing interest in the quest to develop advanced electrocatalysts.[1−7] Addition of another metal to a catalytically active one to form an alloy can alter the availability of active surface sites (ensemble effect)[8] or the binding strength of reactants, intermediates, products, and spectator species (electronic and/or strain effect).[9] Fine tuning of the properties such as particle size, shape, and composition through controlled synthesis of alloy nanomaterials represents a robust approach toward more sophisticated catalysts with enhanced activity,[10,11] selectivity,[12−14] and durability.[15,16]

The oxygen reduction reaction (ORR) is one of the key processes for renewable and environment-compatible schemes of chemical−electrical energy conversion.[17−19] This four-electron electrochemical reaction, $O_2 + 4e^- + 4H^+ \rightarrow 2H_2O$, is usually catalyzed by platinum (Pt) to accelerate the process and conversion of chemical to electrical energy. However, the sluggish kinetics of the ORR requires a substantial amount of this precious metal in real electrochemical systems, which has limited the scaling-up of corresponding renewable energy technologies. Considerable improvement of the catalyst performance for the ORR is demanded to reduce the amount of Pt needed. For example, a 5-fold enhancement of ORR catalytic activity is sought for the commercial implementation of fuel cells in electrical vehicles.[20]

Alloying Pt with 3d transition metals such as Mn, Fe, Ni, Co, and Cu has been demonstrated as a successful approach toward advanced ORR electrocatalysts.[6,21−29] Fundamental studies of well-defined extended surfaces have shown that the enhanced catalytic activity originates from the modified electronic structures of Pt in these alloy catalysts,[5,10,30] which reduces the adsorption of oxygenated spectator species (e.g., OH^-) and thus increases the number of active sites accessible to molecular oxygen. However, it is not straightforward to achieve the same level of activity enhancement in nanocatalysts that are prepared by conventional impregnation or coprecipitation synthesis due to the lack of control over size, homogeneity and shape.[20,31−38] Synthetic methods toward monodisperse and homogeneous alloy nanoparticles (NPs) are thus demanded for systematic studies of these materials for electrocatalysis.

Here, we present a selective summary of recent advances on Pt alloy electrocatalysts for the ORR, with the focus placed on alloy electrocatalysts from organic solution synthesis and their electrocatalytic properties. Although the ORR has broad applications in renewable energy technologies, the emphasis of this review is on the alloy catalysts of platinum and 3d transition metals for proton exchange membrane fuel cells (PEMFCs). The work on extended surfaces, commercial catalysts, or the alloy catalysts prepared by impregnation methods are not covered here, for which comprehensive reviews have already been well documented in the literature.[20,39−42]

SYNTHESIS OF PT ALLOY NANOPARTICLES

The essential challenge for the synthesis of alloy NPs is the diverse nucleation and growth rates of different elements. Typically, Pt salts such as platinum acetylacetonate ($Pt(acac)_2$) have much higher reduction potentials ($Pt^{2+} + 2e^- \leftrightarrow Pt$, E^o = +1.2 V) than 3d transition metals (E^o = −0.2 ∼ −0.4 V). For the synthesis of Pt alloy NPs from a solution, reduction of the Pt precursor is much faster than Fe, Co, Ni, etc. Therefore, the precious metal tends to nucleate first and grow into separate NPs or form Pt-rich regions in the product.[43,44]

The synthesis of conventional Pt-alloy catalysts by impregnation methods[45,46] rely on mixing of high-surface-area Pt/C catalyst with 3d transition metal salt solution, which is

Special Issue: Electrocatalysis

Received: January 31, 2012
Revised: April 4, 2012
Published: April 10, 2012

followed by drying. The formed blends are then subjected to thermal annealing for reduction and alloying. Depending on the precursor ratios and annealing temperatures, the extension of alloying or the level of homogeneity in the catalyst varies by this approach. In addition, high-temperature annealing causes agglomeration of the particles, reduction of specific surface area, and broadening of particle size distribution. This has become the obstacle for application of Pt alloy electrocatalysts in PEMFCs.

Recently, organic solvothermal synthesis has emerged as a powerful approach for making monodisperse and homogeneous alloy nanomaterials.[47−51] This is particularly advantageous in the synthesis of Pt alloy NPs.[44,52−57] Simultaneous growth for alloy NPs has been achieved by coupling the reduction of Pt salts with the decomposition of organometallic precursors of 3d transition metals, usually metal carbonyls, to avoid the mismatch in reduction rate between Pt and 3d metals.[52−55] This has also been done by sequential addition of the precursors so that the salts of the 3d transition metals can be reduced before adding the Pt precursors.[44,54,56,57] The following discussion provides an overview of the progress on synthesis with control over particle size, composition, and shape that has been made by the organic solvothermal approaches.

Particle Size. Multiple parameters in the synthesis can affect the crystal nucleation and growth in solution. To produce monodisperse NPs, it is necessary to have a fast nucleation step followed by a gradual growth process on the formed nuclei, as depicted by the LaMer's plot.[58] Such nucleation can be induced by raising the temperature, or adding the precursor by injection. For the synthesis of alloy NPs, this is usually achieved by addition of the second precursor. When metal carbonyls (e.g., $Mn_2(CO)_{10}$, $Fe(CO)_5$, and $Co_2(CO)_{10}$) are used as precursors for 3d metals, thermal decomposition of the metal carbonyls is fast at elevated temperatures and enables rapid nucleation of the alloy nanocrystals (Figure 1A and B).[52−55] In the case of

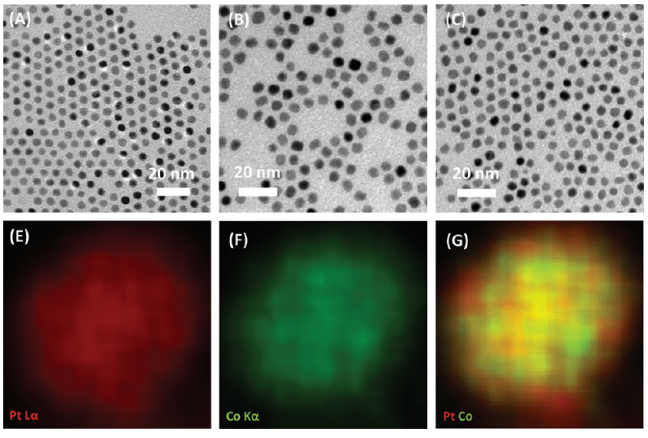

Figure 1. TEM images of the (A) Pt_3Fe, (B) Pt_3Co, and (C) Pt_3Ni NPs from organic solution synthesis. (E−G) Representative EDS elemental maps for a Pt_3Co NP from part B.[54]

metal salts as precursors, such as nickel acetates ($Ni(ac)_2$) for Pt−Ni alloy NPs, the 3d elements have likely been reduced when the Pt precursor is added, and immediate reduction of Pt salts after injection at high temperatures aids the supersaturation of metallic species for fast nucleation (Figure 1C).[44,54,56,57] Element mapping by energy-dispersive X-ray spectroscopy (EDS) based on high-resolution scanning transmission electron microscopy (STEM) has shown that the materials derived from such organic solution syntheses are highly homogeneous alloy NPs, as indicated by the even distribution and good intermixture of Pt and 3d metals in these NPs (Figure 1E−G).[54]

From the growth mechanism described above, it can be seen that the size of alloy NPs is determined by the number of nuclei formed and the amount of precursor remaining in the solution after nucleation. For example, in the synthesis of Pt_3Co NPs with $Pt(acac)_2$ and $Co_2(CO)_{10}$ as precursors,[53,55] the particle size was controlled from <3 to ∼10 nm simply by tuning the temperature at which the cobalt precursor was added (Figure 2). The injection of $Co_2(CO)_{10}$ induced nucleation as the

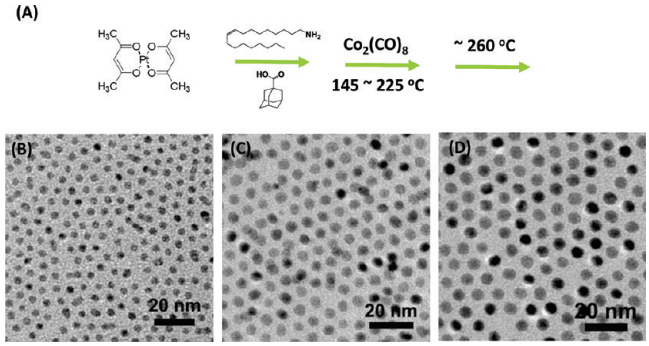

Figure 2. (A) Schematic illustration of the synthetic route for monodisperse Pt_3Co NPs. (B−D) TEM images of the as-synthesized 3, 4.5, and 6 nm Pt_3Co NPs, respectively.[55]

solution color changed from transparent to dark gray immediately. For given amounts of Pt and Co precursors, the higher the temperature for cobalt addition, the more nuclei were generated and the smaller amounts of precursors left in the solution. Therefore, the formed nuclei could only grow into small NPs for adding $Co_2(CO)_{10}$ at high temperatures. In the case of 3 nm Pt_3Co, NPs were obtained when adding $Co_2(CO)_{10}$ at 225 °C, whereas their growth into large NPs became possible when adding $Co_2(CO)_{10}$ at relatively low temperatures (e.g., 9 nm for 145 °C).

Tailoring the balance between the nucleation and growth processes by tuning the growth conditions, such as the initial concentrations of precursors and stabilizing ligands, reaction temperature, and growth time, represents a facile approach toward the synthesis of alloy NPs with controlled size.

Alloy Composition. One advantage of alloy electrocatalysts is the reduced content of Pt metal in the catalyst. Therefore, it is desirable to maximize the content of 3d transition metals in Pt-alloy NPs in order to reduce the cost of materials used as electrocatalyst for the ORR. Moreover, it was found that an increased concentration of alloying elements in subsurface layers substantially alters surface electronic properties and boosts the catalytic performance.[10]

Tuning of the composition of Pt alloy NPs was first achieved by Sun et al. in the synthesis of magnetic FePt NPs,[52] in which the alloy composition was controlled by the ratio between added Fe and Pt precursors. It was found that a 3:2 molar ratio between $Fe(CO)_5$ and $Pt(acac)_2$ gave $Fe_{0.48}Pt_{0.52}$, 2:1 for $Fe_{0.52}Pt_{0.48}$ and 4:1 for $Fe_{0.70}Pt_{0.30}$ NPs. Another example of composition control is the synthesis of Pt_xNi_{1-x} NPs, with Pt_3Ni, PtNi, $PtNi_2$, and $PtNi_3$ NPs obtained with ratios of 1:1.5, 1:2, 1:3.7, and 1:5 between $Pt(acac)_2$ and $Ni(ac)_2$, respectively (Figure 3).[44,57] XRD patterns show that the diffraction peaks of

dx.doi.org/10.1021/cs3000792 | ACS Catal. 2012, 2, 891−898

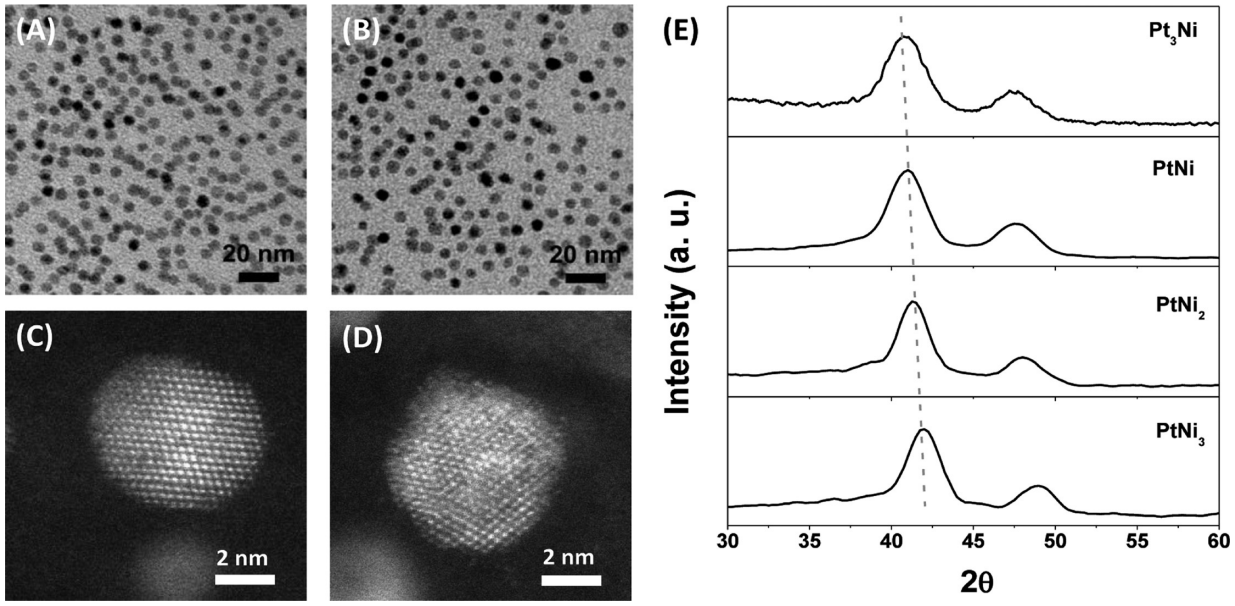

Figure 3. Representative microscopic images of 5 nm Pt_3Ni (A, C) and PtNi (B, D) NPs. (E) XRD patterns of Pt_xNi_{1-x} alloy NPs of various compositions, with the positions of the (111) peak labeled by a dashed line.[57]

these alloy NPs monotonically shift toward a high angle as the ratio of Ni increases, indicating that the dependence of lattice constant on the alloy composition follows the Vegard's law.

On that basis, it is obvious that excessive amounts of 3d metal precursors are needed in the synthesis of Pt alloy NPs. This could be due to the rather high nucleation threshold concentration or low reduction rate of the 3d elements. Elemental analysis of the growth solution after separation of the product NPs usually shows the presence of 3d metals, whereas Pt residues are rarely observed. It is also interesting to point out that composition control has not been achieved for Pt−Co alloy NPs. So far, only Pt_3Co NPs have been obtained. This is likely caused by the specific pathway for the decomposition of $Co_2(CO)_5$,[59] but there is no clue as yet for the syntheses with cobalt salts as precursors.[60] A similar argument also holds true for Pt−Mn NPs.[61]

Shape Control. Shape-controlled growth of nanocrystals has been pursued for the development of advanced catalysts for more than a decade.[62−65] NPs of controlled shapes can have only one type of facet on the surface (e.g., cube with (100) and octahedron with (111)), and, thus, enable comparative studies of nanocatalysts versus extended surfaces of single crystals. Although the synthesis of Pt NPs with shape control has been achieved in early studies,[62] it is more challenging for Pt-based alloys, and only until very recently has certain progress been made for Pt_3M systems.[61,66−69] In the synthesis of alloy NPs, the presence of two or more types of elements with different growth kinetics, surface energies, and binding strengths to surfactants makes it challenging to control the crystal growth along different crystalline directions. Since (111) has the lowest surface energy among the low-index facets, fcc crystals tend to grow along the ⟨100⟩ direction into an octahedron-like shape. However, the lack of sufficient thermodynamically controlled growth after the consumption of precursors by the short nucleation burst usually results in cuboctahedral or truncated octahedral NPs (enclosed by both (111) and (100) facets).[25,70−72] To induce anisotropic growth into the desired shapes of single-facet surface, additional factors have to be introduced.

Two strategies have been developed to effectively control the growth of Pt alloy NPs into cubic or octahedral shapes. Zhang et al. introduced tungsten as an intermediate by adding tungsten carbonyl ($W(CO)_6$) into their synthesis of alloy NPs. It was believed that tungsten served as a decelerator for the growth dynamics through a "buffer" mechanism. Tungsten carbonyl readily decomposed to give elemental tungsten substances and provide the initial reduction of Pt salts through $Pt^{2+} + W \leftrightarrow W^{n+} + Pt$ for nanocrystal nucleation. As the amount of tungsten cations accumulated in the solution, the equilibrium of this galvanic reaction slowed down the rate of reduction and, thus, the nucleation/growth speed, enabling thermodynamic growth into octahedrons. By this strategy, they have been able to obtain octahedral Pt_3Ni NPs (Figure 4).[68]

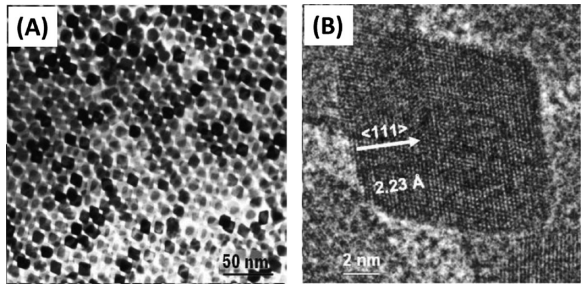

Figure 4. (A) TEM and (B) HRTEM images of octahedral Pt_3Ni NPs synthesized with $W(CO)_6$ as "buffer".[68]

Another group, Wu et al., used CO as a gas reducing agent and obtained cubic Pt-alloy NPs (Figure 5).[69] Instead of inert gas typically employed in organic solvothermal synthesis, they carried out nanocrystal growth under a reductive atmosphere. It was claimed that the shape control was in place due to the stronger adsorption of CO on (100) than on (111) of Pt surfaces,[73] which induced the preferential growth along ⟨111⟩ directions into cubes.

Despite the statements claimed therein (as discussed above), questions about the growth mechanisms are still present for

dx.doi.org/10.1021/cs3000792 | ACS Catal. 2012, 2, 891−898

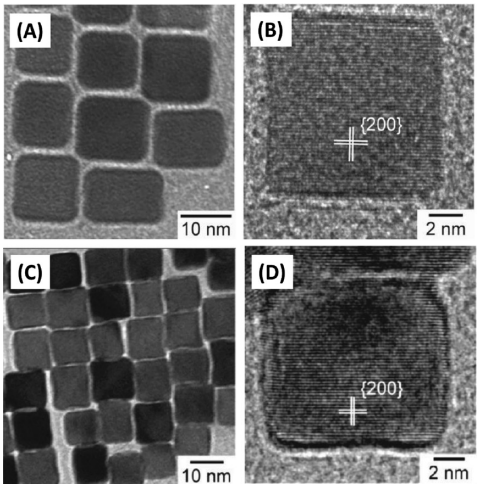

Figure 5. Microscopic images of (A, B) Pt_3Ni and (C, D) Pt_3Co nanocubes synthesized with CO as reducing gas.[69]

these studies. Considering the decomposition of $W(CO)_6$ also produces CO, the strong adsorption of CO on Pt(100) is likely competing with the thermodynamic driving forces for growth along ⟨100⟩ directions in the first report.[68] In the other work, CO is also a reducing agent for Pt cations, and the preferentially adsorbed CO on Pt (100) is not only a blocking agent but also active sites for deposition of Pt atoms.[69] More comprehensive studies of the growth mechanisms underlying these primary reports could provide the clue for rational design of NP synthesis with shape control.

ELECTROCATALYTIC PERFORMANCE OF PT ALLOY NANOCATALYSTS

Advancement on the controlled synthesis of monodisperse and homogeneous Pt alloy NPs has enabled the systematic studies of these materials for catalytic applications. In the following, we first describe the preparation of electrocatalysts from colloidal NPs and then explain the relationship between the Pt alloy nanostructures and their electrocatalytic performance in terms of particle size, shape, and composition.

Catalyst Preparation and Pretreatment. The NPs processed from organic solution synthesis cannot be directly applied as catalysts. Generally, they are deposited onto a high-surface-area support, such as carbon black, and then subjected to pretreatments for cleaning and surfactant removal. The as-synthesized Pt alloy NPs are usually capped by oleylamine or oleic acid (or both) ligands.[44,52−57,61,66−69] Although these ligands stabilize the NPs in solution and help control the size and shape in nanocrystal growth, they are detrimental for catalysis because they block the access of reactant molecules to the surface atoms.

Several methods have been developed to remove the organic ligands and clean the surface for application of colloidal NPs. It was found that the surfactants can be oxidized by mild heating (160−200 °C) in an oxygenated atmosphere.[55,74] TEM studies confirmed that no particle aggregation or agglomeration occurred after the treatment.[54,57] The treated catalysts show consistent improvements in electrocatalytic activity compared to the corresponding extended surfaces.[54] Other methods include chemical washing by tetramethylammonium hydroxide[75] or acetic acid[76] and UV ozone[77] treatment. Although all of these methods have been shown to be capable of cleaning the surface of Pt and Pt alloy nanocatalysts, the efficiencies differ, and comprehensive studies about the chemical mechanisms of these treatments are still missing.

Thermal annealing is another important pretreatment in alloy catalyst preparation. This is usually carried out in vacuum or a reducing atmosphere (H_2, CO, etc.), and the primary purpose is to improve the alloy homogeneity. For Pt alloy electrocatalysts, annealing may also induce surface segregation that results in beneficial surface properties for the ORR;[5,10,78] however, annealing may also induce sintering of NPs. The loss of consistency in particle size has made it ambiguous to deduce the intrinsic annealing effect.[32,79,80] The monodisperse and homogeneous alloy NPs obtained by organic solvothermal synthesis, however, have enabled systematic studies of the annealing effect on the catalytic performance of Pt alloy electrocatalysts.

Figure 6 shows the TEM images of the Pt_3Co/C catalysts after annealing at various temperatures. The catalyst was made

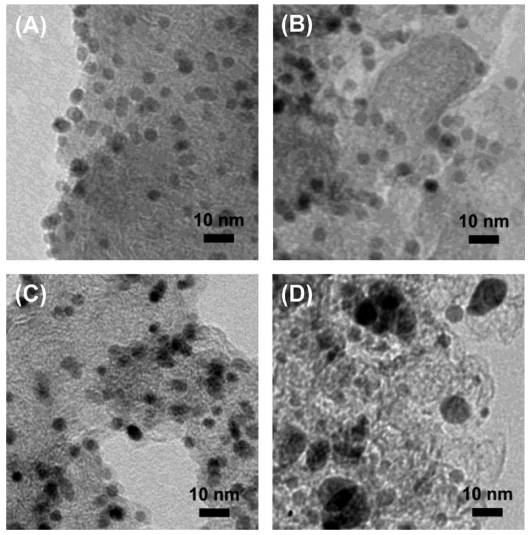

Figure 6. TEM images of (A) as-prepared and (b) 400 °C, (c) 500 °C, and (d) 800 °C annealed 4.5 nm Pt_3Co/C catalysts.[81]

with 4.5 nm alloy NPs processed from organic solution synthesis (as shown in Figure 2C).[81] The as-prepared catalyst (Figure 6A) was annealed in Ar + 5% H_2 for a temperature range from 300 to 800 °C. No obvious size or morphology change was observed for the catalysts annealed up to 400 °C (Figure 6B). Particle sintering started to appear for annealing at 500 °C, but yet, not significantly so at this temperature (Figure 6C). Substantial agglomeration was observed for annealing above 600 °C (Figure 6D). In the latter case, large particles of more than 20 nm appeared. Electrochemical studies show that the electrochemically active surface area decreases and the specific catalytic activity increases as the annealing temperature escalates (Figure 7A). These transitions are a reflection of both surface restructuring (smoothing, surface segregation, etc.) and particle sintering, which were dominant for low (<500 °C) and high (>500 °C) temperature annealing, respectively. An important finding from this temperature-dependent study is that the optimal treating conditions for the maximal mass activity is 400−500 °C for such alloy nanocatalysts (Figure 7B).

Particle Size Effect. The particle size effect for Pt electrocatalysts has been well documented in the literature[20,82,83] and explained in terms of the surface geometry

dx.doi.org/10.1021/cs3000792 | ACS Catal. 2012, 2, 891−898

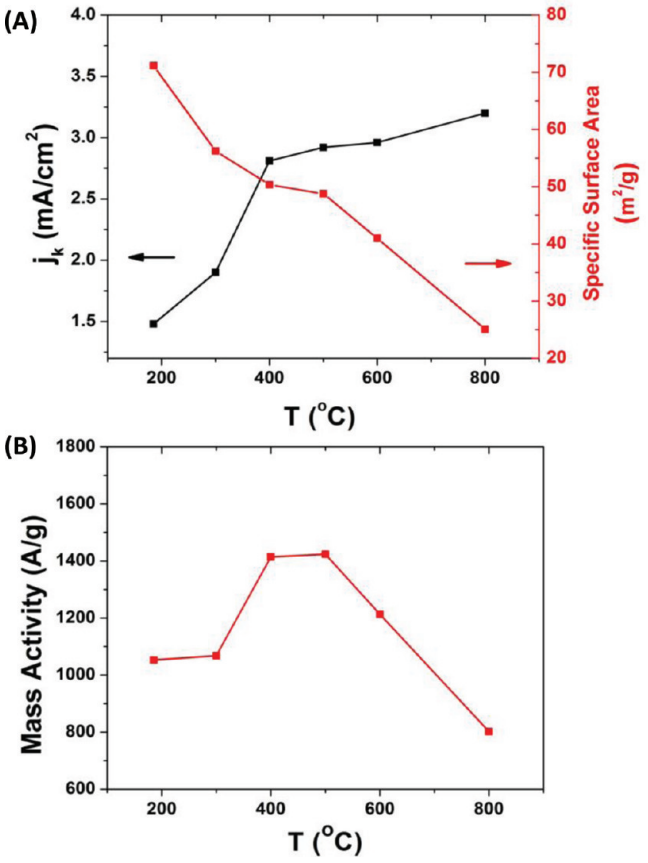

Figure 7. Annealing temperature-dependent electrocatalytic performance of 4.5 nm Pt_3Co/C catalysts for the ORR. (A) The dependence of specific activity and specific surface area on the annealing temperature. (B) The plot of mass activity vs the annealing temperature.[81]

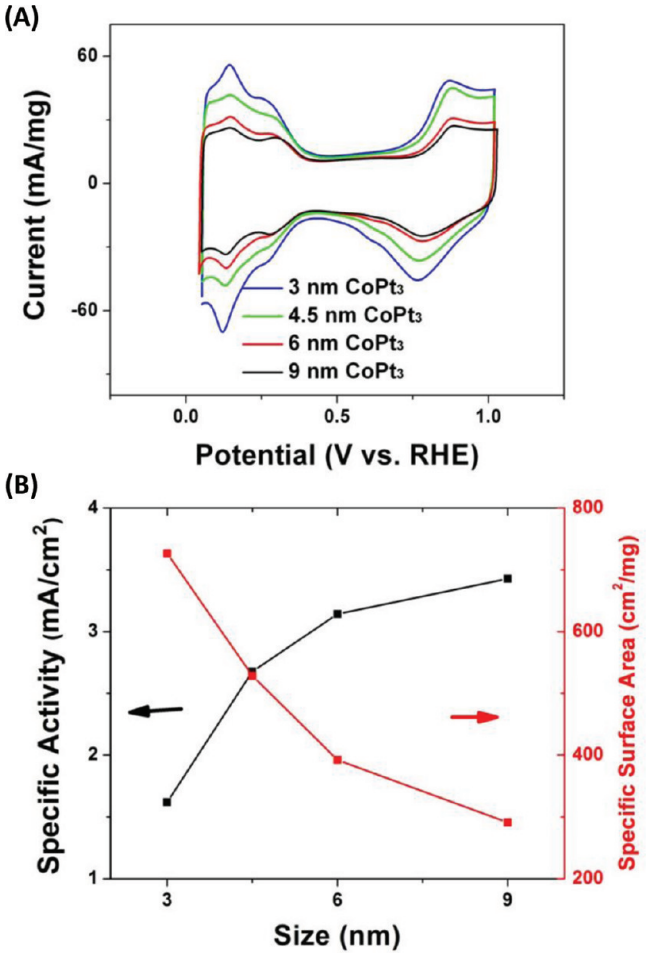

Figure 8. Size-dependent electrocatalytic performance of Pt alloy nanocatalysts. (A) CVs of Pt_3Co/C catalysts with Pt_3Co NPs of different sizes. (B) Specific activities (black, at 0.9 V vs RHE) and specific surface areas (red) of the Pt_3Co/C catalysts depending on particle size.[55]

and associated electronic properties, with enhanced adsorption of oxygenated species (O^- and OH_{ad}, etc.) on smaller particles due to their smaller average surface coordination numbers and consequently more pronounced oxophilic behavior,[84] which block the access of molecular oxygen. Systematic study of Pt alloy nanocatalysts of various sizes demonstrated that a particle size effect is also present in alloy catalysts.[55] Cyclic voltammograms (CVs) for the Pt_3Co/C catalysts with particle size ranging from 3 to 9 nm show that the H_{upd} peaks (0.05 V < E < 0.4 V vs RHE) shrink as the particle size increases as a result of the decrease in specific surface area (Figure 8A). Both the oxidation peak (~0.9 V) in the anodic scan and the reduction peak (~0.8 V) in the cathodic scan exhibit positive shifts with increasing particle size, indicating smaller NPs are more oxophilic than bigger ones because of the higher ratio of undercoordinated atoms (edge and corner sites) on the surface.[82] Correspondingly, the specific activity for the ORR also increases with the particle size (Figure 8B), and as a result, the optimal size for the maximum in mass activity was established to be around 4.5 nm.

Shape Effect. Model catalyst studies of well-defined extended surfaces have revealed that the electrocatalytic performance of Pt alloy catalysts is sensitive to the surface structures.[5,10,78] For single-crystal surfaces of Pt_3Ni, the electrocatalytic activity for the ORR follows the order (111) ≫ (110) > (100). The Pt_3Ni(111) surface was found to form a Pt skin by surface segregation after ultrahigh vacuum (UHV) annealing, which shows improvement factors of more than an order of magnitude versus Pt(111) or polycrystalline Pt (poly-Pt).[10] This has inspired the search for octahedral Pt alloy nanocatalysts, which are enclosed by {111} facets only, and it is hoped that the same level of activity enhancement can be achieved in nanocatalysts as on extended surfaces.

Electrocatalytic performance of octahedral Pt_3Ni NPs has been studied on the basis of alloy NPs (Figure 4) processed from organic solvothermal synthesis.[68] Substantially enhanced ORR catalytic activity was observed for the alloy catalyst made of octahedral Pt_3Ni NPs versus commercial Pt/C (Figure 9). Considering the effect of particle size on electrocatalytic performance as discussed above, it has to be pointed out that the benchmark Pt/C catalyst used in this study had an average particle size 3 times smaller than the Pt_3Ni octahedrons. It should also be noted that the studied Pt_3Ni nanocatalysts may only have a Pt-skeleton surface, rather than the Pt skin as achieved on extended surfaces.[10]

Composition Effect and Surface Chemistry. The relationship between electrocatalytic activity and alloy composition for Pt-alloy catalysts does not follow a simple monotonic trend, but instead, a volcano-like dependence. It was revealed in Pt_xNi_{1-x}/C catalysts that an intermediate composition, close to a 1:1 ratio between Pt and Ni, gave the

dx.doi.org/10.1021/cs3000792 | ACS Catal. 2012, 2, 891–898

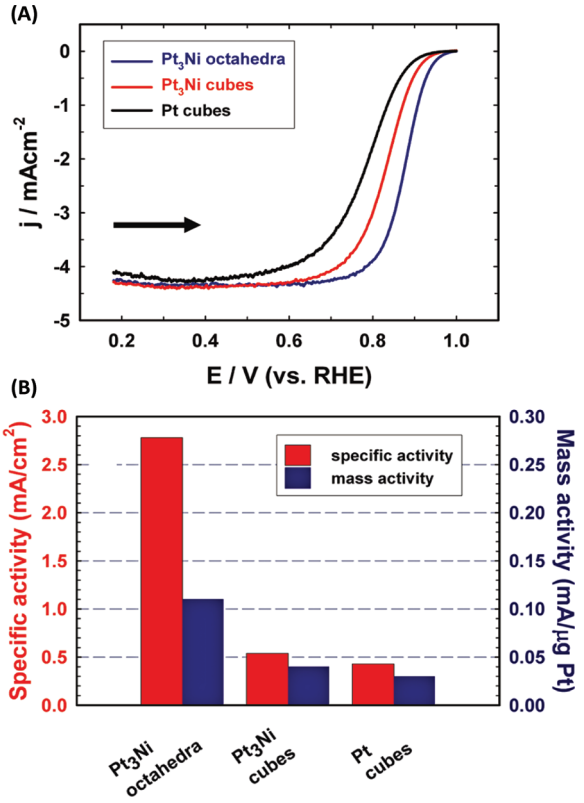

Figure 9. Shape effect on the electrocatalytic activity of Pt alloy nanocatalysts. (A) Polarization curves and (B) summary of specific and mass activities for Pt_3Ni/C catalysts with NPs of octahedral and cubic shapes.[68]

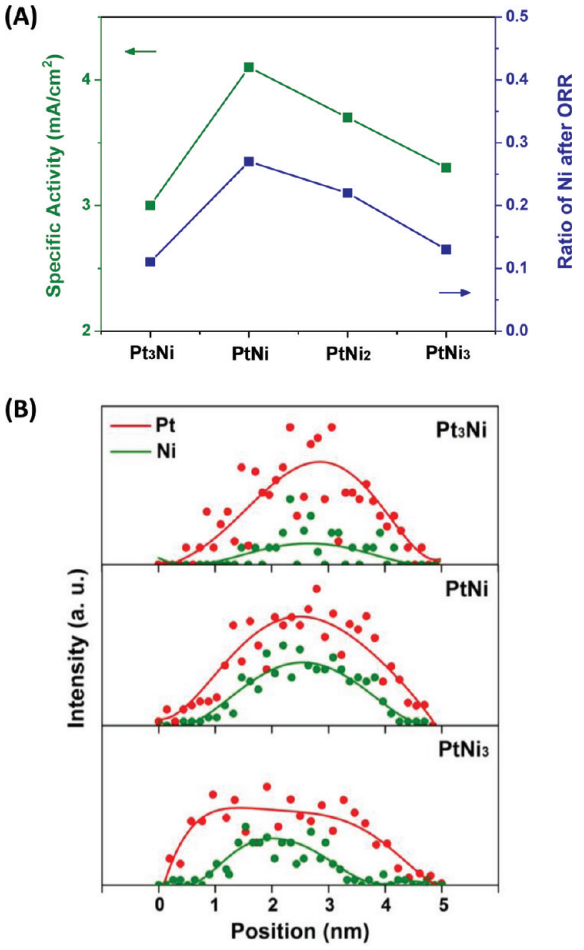

Figure 10. Composition dependence studies of Pt alloy electrocatalysts. (A) The dependence of ORR catalytic activity and the ratio of Ni preserved after electrochemical measurements on the alloy initial composition for the Pt_xNi_{1-x}/C nanocatalysts. (B) Composition line profiles for the Pt_xNi_{1-x}/C nanocatalysts after ORR measurements.[57]

highest ORR catalytic activity (Figure 10A).[57] This turned down the hope to have as much 3d metal as possible in the alloy catalyst for reduction of system cost.

It is known that the 3d metal atoms present on the surface are leached out when the alloy catalysts are exposed to the acidic electrochemical environment, and a skeleton type of surface structure is formed.[5,78,85] EDS analysis for the Pt_xNi_{1-x}/C catalysts after electrochemical measurements revealed that the alloy composition had significant changes, with less Ni in the catalysts than the as-synthesized NPs. For example, the average Ni composition in the PtNi/C (Pt/Ni = 1:1) catalyst was found to be 27% after the ORR measurement. The ratio of Ni left also possessed a volcano-shape dependence on the initial alloy composition, coinciding with the trend of catalytic activity (Figure 10A).[57] These results demonstrate that the extent of leaching by acid and, hence, the thickness of Pt skeleton structure on the surface are regulated by the initial alloy composition.

Further detailed characterization of the compositional profiles for these alloy catalysts by EDS based on aberration-corrected high-angle annular dark field STEM provided strong evidence for these arguments (Figure 10B). It was shown that all the measured alloy catalysts had an alloy core surrounded by a Pt-rich shell, with the Pt/Ni ratios of the core consistent with the initial compositions of the alloy catalysts. The thickness of the Pt shell, however, varies for different initial alloy compositions. For example, the thickness is over 1 nm (at half-maximum) for the $PtNi_3$/C, versus ~0.5 nm for PtNi/C after ORR. It was thus concluded that electrocatalytic performance of the Pt alloy catalysts depends on the remaining ratio of the 3d metal in the catalyst and the thickness of the Pt skeleton overlayer formed after depletion of the 3d metal from the surface.

FUTURE DIRECTIONS

Recent advancement in the synthesis and electrocatalytic properties of platinum−3d transition metal alloy catalysts for the oxygen reduction reaction has been reviewed. The development of organic solution synthesis with monodisperse and homogeneous alloy nanoparticles has enabled systematic studies of these alloy materials for electrocatalytic applications. Critical parameters such as particle size, shape and composition have been investigated and tailored for catalytic activity enhancement. These studies plus further optimization of surface structures[78] could eventually lead to advanced electrocatalysts and electrochemical systems suitable for large-scale applications. Even though significant progress has been made, there is still a lack of complete fundamental understanding of material properties at nanoscale. For that reason, it is expected that further development of ex situ and in situ techniques will provide detailed insight into critical properties of nanoparticles that determine their catalytic performance. In situ HRTEM under ambient conditions may resolve how topmost atoms of the catalyst behave under reaction-relevant conditions.[86]

dx.doi.org/10.1021/cs3000792 | ACS Catal. 2012, 2, 891−898

Moreover, the possibility to tune the exact environment can provide invaluable information about catalyst−reactant interactions at the atomic scale. Great expectations are placed on electrochemical in situ TEM,[87] which has the ability to follow processes that may be responsible for dissolution of the particles, and therefore, this technique will be crucial for addressing issues related to the stability of the catalysts.

Despite the rapid development in TEM techniques, it still remains a challenge to perform surface specific analyses at nanoscale. Development of such techniques would have tremendous impact on heterogeneous catalysis. That would enable detection and control of segregation processes as well as detailed surface structure and surface composition characterizations. As of now, there is a lack of techniques that can address these issues for nanoscale materials. For instance, HR-SEM and low-energy electron microscopy continue to improve in promising directions;[88,89] however, further improvements are expected in both.

In addition to advanced microscopy tools, it is possible to rely on synergy between techniques that are surface-specific, such as spectroelectrochemical infrared measurements.[90] In such an approach, one could eventually use infrared spectra obtained in reflective mode during electrochemical reaction to reveal bond -making and -breaking processes that can be assigned to specific surface features, structure, and composition. All of these represent a great challenge, and the field of electrocatalysis will strongly rely on the advancements that will be made in the near future.

AUTHOR INFORMATION

Corresponding Author

*E-mail: vrstamenkovic@anl.gov.

Notes

The authors declare no competing financial interest.

ACKNOWLEDGMENTS

This work was conducted at Argonne National Laboratory, a U.S. Department of Energy, Office of Science Laboratory, operated by UChicago Argonne, LLC, under contract no. DE-AC02-06CH11357. This research was sponsored by the U.S. Department of Energy, Office of Energy Efficiency and Renewable Energy, Fuel Cell Technologies Program.

REFERENCES

(1) Besenbacher, F.; Chorkendorff, I.; Clausen, B. S.; Hammer, B.; Molenbroek, A. M.; Norskov, J. K.; Stensgaard, I. *Science* **1998**, *279*, 1913−1915.
(2) Diemant, T.; Hager, T.; Hoster, H. E.; Rauscher, H.; Behm, R. J. *Surf. Sci.* **2003**, *541*, 137−146.
(3) Greeley, J.; Mavrikakis, M. *Nat. Mater.* **2004**, *3*, 810−815.
(4) Chen, M. S.; Kumar, D.; Yi, C. W.; Goodman, D. W. *Science* **2005**, *310*, 291−293.
(5) Stamenkovic, V. R.; Mun, B. S.; Arenz, M.; Mayrhofer, K. J. J.; Lucas, C. A.; Wang, G. F.; Ross, P. N.; Markovic, N. M. *Nat. Mater.* **2007**, *6*, 241−247.
(6) Strasser, P.; Koh, S.; Anniyev, T.; Greeley, J.; More, K.; Yu, C. F.; Liu, Z. C.; Kaya, S.; Nordlund, D.; Ogasawara, H.; Toney, M. F.; Nilsson, A. *Nat. Chem.* **2010**, *2*, 454−460.
(7) Tao, F.; Grass, M. E.; Zhang, Y. W.; Butcher, D. R.; Aksoy, F.; Aloni, S.; Altoe, V.; Alayoglu, S.; Renzas, J. R.; Tsung, C. K.; Zhu, Z. W.; Liu, Z.; Salmeron, M.; Somorjai, G. A. *J. Am. Chem. Soc.* **2010**, *132*, 8697−8703.
(8) Maroun, F.; Ozanam, F.; Magnussen, O. M.; Behm, R. J. *Science* **2001**, *293*, 1811−1814.
(9) Burch, R. *Acc. Chem. Res.* **1982**, *15*, 24−31.
(10) Stamenkovic, V. R.; Fowler, B.; Mun, B. S.; Wang, G. F.; Ross, P. N.; Lucas, C. A.; Markovic, N. M. *Science* **2007**, *315*, 493−497.
(11) Studt, F.; Abild-Pedersen, F.; Bligaard, T.; Sorensen, R. Z.; Christensen, C. H.; Norskov, J. K. *Science* **2008**, *320*, 1320−1322.
(12) Jankowiak, J. T.; Barteau, M. A. *J. Catal.* **2005**, *236*, 366−378.
(13) Linic, S.; Jankowiak, J.; Barteau, M. A. *J. Catal.* **2004**, *224*, 489−493.
(14) Kesavan, L.; Tiruvalam, R.; Ab Rahim, M. H.; bin Saiman, M. I.; Enache, D. I.; Jenkins, R. L.; Dimitratos, N.; Lopez-Sanchez, J. A.; Taylor, S. H.; Knight, D. W.; Kiely, C. J.; Hutchings, G. J. *Science* **2011**, *331*, 195−199.
(15) Greeley, J.; Stephens, I. E. L.; Bondarenko, A. S.; Johansson, T. P.; Hansen, H. A.; Jaramillo, T. F.; Rossmeisl, J.; Chorkendorff, I.; Norskov, J. K. *Nat. Chem.* **2009**, *1*, 552−556.
(16) Wang, C.; van der Vliet, D.; More, K. L.; Zaluzec, N. J.; Peng, S.; Sun, S. H.; Daimon, H.; Wang, G. F.; Greeley, J.; Pearson, J.; Paulikas, A. P.; Karapetrov, G.; Strmcnik, D.; Markovic, N. M.; Stamenkovic, V. R. *Nano Lett.* **2011**, *11*, 919−926.
(17) Vielstich, W.; Lamm, A.; Gasteiger, H. A. *Handbook of Fuel Cells: Fundamentals, Technology, And Applications*; Wiley: Chichester, England, Hoboken, NJ, 2003.
(18) Abraham, K. M.; Jiang, Z. *J. Electrochem. Soc.* **1996**, *143*, 1−5.
(19) Armand, M.; Tarascon, J. M. *Nature* **2008**, *451*, 652−657.
(20) Gasteiger, H. A.; Kocha, S. S.; Sompalli, B.; Wagner, F. T. *Appl. Catal., B* **2005**, *56*, 9−35.
(21) Toda, T.; Igarashi, H.; Uchida, H.; Watanabe, M. *J. Electrochem. Soc.* **1999**, *146*, 3750−3756.
(22) Scott, R. W. J.; Wilson, O. M.; Oh, S. K.; Kenik, E. A.; Crooks, R. M. *J. Am. Chem. Soc.* **2004**, *126*, 15583−15591.
(23) Hernandez, J.; Solla-Gullon, J.; Herrero, E.; Aldaz, A.; Feliu, J. M. *J. Phys. Chem. C* **2007**, *111*, 14078−14083.
(24) Zhang, J.; Sasaki, K.; Sutter, E.; Adzic, R. R. *Science* **2007**, *315*, 220−222.
(25) Wang, C.; Daimon, H.; Onodera, T.; Koda, T.; Sun, S. H. *Angew. Chem., Int. Ed.* **2008**, *47*, 3588−3591.
(26) Wang, J. X.; Inada, H.; Wu, L. J.; Zhu, Y. M.; Choi, Y. M.; Liu, P.; Zhou, W. P.; Adzic, R. R. *J. Am. Chem. Soc.* **2009**, *131*, 17298−17302.
(27) Ataee-Esfahani, H.; Wang, L.; Nemoto, Y.; Yamauchi, Y. *Chem. Mater.* **2010**, *22*, 6310−6318.
(28) Li, W. Z.; Chen, Z. W.; Xu, L. B.; Yan, Y. S. *J. Power Sources* **2010**, *195*, 2534−2540.
(29) Mazumder, V.; Chi, M. F.; More, K. L.; Sun, S. H. *Angew. Chem., Int. Ed.* **2010**, *49*, 9368−9372.
(30) Stamenkovic, V.; Mun, B. S.; Mayrhofer, K. J. J.; Ross, P. N.; Markovic, N. M.; Rossmeisl, J.; Greeley, J.; Norskov, J. K. *Angew. Chem., Int. Ed.* **2006**, *45*, 2897−2901.
(31) Mukerjee, S.; Srinivasan, S. *J. Electroanal. Chem.* **1993**, *357*, 201−224.
(32) Mukerjee, S.; Srinivasan, S.; Soriaga, M. P.; Mcbreen, J. *J. Phys. Chem.* **1995**, *99*, 4577−4589.
(33) Min, M. K.; Cho, J. H.; Cho, K. W.; Kim, H. *Electrochim. Acta* **2000**, *45*, 4211−4217.
(34) Paulus, U. A.; Wokaun, A.; Scherer, G. G.; Schmidt, T. J.; Stamenkovic, V.; Markovic, N. M.; Ross, P. N. *Electrochim. Acta* **2002**, *47*, 3787−3798.
(35) Paulus, U. A.; Wokaun, A.; Scherer, G. G.; Schmidt, T. J.; Stamenkovic, V.; Radmilovic, V.; Markovic, N. M.; Ross, P. N. *J. Phys. Chem. B* **2002**, *106*, 4181−4191.
(36) Soderberg, J. N.; Sirk, A. H. C.; Campbell, S. A.; Birss, V. I. *J. Electrochem. Soc.* **2005**, *152*, A2017−A2022.
(37) Qian, Y. D.; Wen, W.; Adcock, P. A.; Jiang, Z.; Hakim, N.; Saha, M. S.; Mukerjee, S. *J. Phys. Chem. C* **2008**, *112*, 1146−1157.
(38) Hwang, B. J.; Kumar, S. M. S.; Chen, C. H.; Monalisa; Cheng, M. Y.; Liu, D. G.; Lee, J. F. *J. Phys. Chem. C* **2007**, *111*, 15267−15276.
(39) Bing, Y. H.; Liu, H. S.; Zhang, L.; Ghosh, D.; Zhang, J. J. *Chem. Soc. Rev.* **2010**, *39*, 2184−2202.

(40) Markovic, N. M.; Schmidt, T. J.; Stamenkovic, V.; Ross, P. N. *Fuel Cells* **2001**, *1*, 105−116.
(41) Strasser, P. *Rev. Chem. Eng.* **2009**, *25*, 255−295.
(42) Markovic, N. M.; Ross, P. N. *Surf. Sci. Rep.* **2002**, *45*, 121−229.
(43) Chen, M.; Liu, J. P.; Sun, S. H. *J. Am. Chem. Soc.* **2004**, *126*, 8394−8395.
(44) Ahrenstorf, K.; Heller, H.; Kornowski, A.; Broekaert, J. A. C.; Weller, H. *Adv. Funct. Mater.* **2008**, *18*, 3850−3856.
(45) Ponec, V.; Bond, G. C. *Catalysis by Metals and Alloys*; Elsevier: Amsterdam, New York, 1995.
(46) Ertl, G.; Knözinger, H.; Weitkamp, J. *Handbook of Heterogeneous Catalysis*. VCH: Weinheim, 1997.
(47) Murray, C. B.; Kagan, C. R.; Bawendi, M. G. *Annu. Rev. Mater. Sci.* **2000**, *30*, 545−610.
(48) Cushing, B. L.; Kolesnichenko, V. L.; O'Connor, C. J. *Chem. Rev.* **2004**, *104*, 3893−3946.
(49) Ferrando, R.; Jellinek, J.; Johnston, R. L. *Chem. Rev.* **2008**, *108*, 845−910.
(50) Guo, S. J.; Wang, E. K. *Nano Today* **2011**, *6*, 240−264.
(51) Cuenya, B. R. *Thin Solid Films* **2010**, *518*, 3127−3150.
(52) Sun, S. H.; Murray, C. B.; Weller, D.; Folks, L.; Moser, A. *Science* **2000**, *287*, 1989−1992.
(53) Shevchenko, E. V.; Talapin, D. V.; Rogach, A. L.; Kornowski, A.; Haase, M.; Weller, H. *J. Am. Chem. Soc.* **2002**, *124*, 11480−11485.
(54) Wang, C.; Chi, M. F.; Li, D. G.; van der Vliet, D.; Wang, G. F.; Lin, Q. Y.; Mitchell, J. F.; More, K. L.; Markovic, N. M.; Stamenkovic, V. R. *ACS Catal.* **2011**, *1*, 1355−1359.
(55) Wang, C.; van der Vilet, D.; Chang, K. C.; You, H. D.; Strmcnik, D.; Schlueter, J. A.; Markovic, N. M.; Stamenkovic, V. R. *J. Phys. Chem. C* **2009**, *113*, 19365−19368.
(56) Ahrenstorf, K.; Albrecht, O.; Heller, H.; Kornowski, A.; Gorlitz, D.; Weller, H. *Small* **2007**, *3*, 271−274.
(57) Wang, C.; Chi, M. F.; Wang, G. F.; van der Vliet, D.; Li, D. G.; More, K.; Wang, H. H.; Schlueter, J. A.; Markovic, N. M.; Stamenkovic, V. R. *Adv. Funct. Mater.* **2011**, *21*, 147−152.
(58) LaMer, V. K.; Dinegar, R. H. *J. Am. Chem. Soc.* **1950**, *72*, 4847−4854.
(59) Shevchenko, E. V.; Talapin, D. V.; Schnablegger, H.; Kornowski, A.; Festin, O.; Svedlindh, P.; Haase, M.; Weller, H. *J. Am. Chem. Soc.* **2003**, *125*, 9090−9101.
(60) Zhang, J.; Fang, J. Y. *J. Am. Chem. Soc.* **2009**, *131*, 18543−18547.
(61) Kang, Y. J.; Murray, C. B. *J. Am. Chem. Soc.* **2010**, *132*, 7568−7569.
(62) Ahmadi, T. S.; Wang, Z. L.; Green, T. C.; Henglein, A.; El-Sayed, M. A. *Science* **1996**, *272*, 1924−1926.
(63) Chen, J. Y.; Lim, B.; Lee, E. P.; Xia, Y. N. *Nano Today* **2009**, *4*, 81−95.
(64) Peng, Z. M.; Yang, H. *Nano Today* **2009**, *4*, 143−164.
(65) Burda, C.; Chen, X. B.; Narayanan, R.; El-Sayed, M. A. *Chem. Rev.* **2005**, *105*, 1025−1102.
(66) Chen, M.; Kim, J.; Liu, J. P.; Fan, H. Y.; Sun, S. H. *J. Am. Chem. Soc.* **2006**, *128*, 7132−7133.
(67) Liu, Q. S.; Yan, Z.; Henderson, N. L.; Bauer, J. C.; Goodman, D. W.; Batteas, J. D.; Schaak, R. E. *J. Am. Chem. Soc.* **2009**, *131*, 5720−5721.
(68) Zhang, J.; Yang, H. Z.; Fang, J. Y.; Zou, S. Z. *Nano Lett.* **2010**, *10*, 638−644.
(69) Wu, J. B.; Gross, A.; Yang, H. *Nano Lett.* **2011**, *11*, 798−802.
(70) Wang, Z. L. *J. Phys. Chem. B* **2000**, *104*, 1153−1175.
(71) Wang, C.; Daimon, H.; Lee, Y.; Kim, J.; Sun, S. *J. Am. Chem. Soc.* **2007**, *129*, 6974−6975.
(72) Ren, J. T.; Tilley, R. D. *J. Am. Chem. Soc.* **2007**, *129*, 3287−3291.
(73) Eichler, A. *Surf. Sci.* **2002**, *498*, 314−320.
(74) Liu, Z. F.; Shamsuzzoha, M.; Ada, E. T.; Reichert, W. M.; Nikles, D. E. *J. Power Sources* **2007**, *164*, 472−480.
(75) Liu, Z. F.; Ada, E. T.; Shamsuzzoha, M.; Thompson, G. B.; Nikles, D. E. *Chem. Mater.* **2006**, *18*, 4946−4951.
(76) Lee, Y. H.; Lee, G.; Shim, J. H.; Hwang, S.; Kwak, J.; Lee, K.; Song, H.; Park, J. T. *Chem. Mater.* **2006**, *18*, 4209−4211.
(77) Chen, W.; Kim, J. M.; Sun, S. H.; Chen, S. W. *J. Phys. Chem. C* **2008**, *112*, 3891−3898.
(78) Wang, C.; Chi, M. F.; Li, D. G.; Strmcnik, D.; van der Vliett, D.; Wang, G. F.; Komanicky, V.; Chang, K. C.; Paulikas, A. P.; Tripkovic, D.; Pearson, J.; More, K. L.; Markovic, N. M.; Stamenkovic, V. R. *J. Am. Chem. Soc.* **2011**, *133*, 14396−14403.
(79) Liu, H.; Li, W.; Manthiram, A. *Appl. Catal., B* **2009**, *90*, 184−194.
(80) Schulenburg, H.; Muller, E.; Khelashvili, G.; Roser, T.; Bonnemann, H.; Wokaun, A.; Scherer, G. G. *J. Phys. Chem. C* **2009**, *113*, 4069−4077.
(81) Wang, C.; Wang, G. F.; van der Vliet, D.; Chang, K. C.; Markovic, N. M.; Stamenkovic, V. R. *Phys. Chem. Chem. Phys.* **2010**, *12*, 6933−6939.
(82) Kinoshita, K. *J. Electrochem. Soc.* **1990**, *137*, 845−848.
(83) Mayrhofer, K. J. J.; Blizanac, B. B.; Arenz, M.; Stamenkovic, V. R.; Ross, P. N.; Markovic, N. M. *J. Phys. Chem. B* **2005**, *109*, 14433−14440.
(84) Han, B. C.; Miranda, C. R.; Ceder, G. *Phys. Rev. B* **2008**, 77.
(85) Stamenkovic, V. R.; Mun, B. S.; Mayrhofer, K. J. J.; Ross, P. N.; Markovic, N. M. *J. Am. Chem. Soc.* **2006**, *128*, 8813−8819.
(86) Gai, P. L. *Microsc. Microanal.* **2002**, *8*, 21−28.
(87) Dolle, M.; Grugeon, S.; Beaudoin, B.; Dupont, L.; Tarascon, J. M. *J. Power Sources* **2001**, *97*−*8*, 104−106.
(88) Bogner, A.; Jouneau, P. H.; Thollet, G.; Basset, D.; Gauthier, C. *Micron* **2007**, *38*, 390−401.
(89) Schatten, H. *Micron* **2011**, *42*, 175−185.
(90) Dunsch, L. *J. Solid State Electrochem.* **2011**, *15*, 1631−1646.